Seasonal salt budget of the northwestern tropical Atlantic Ocean along 38°W

Gregory R. Foltz,[1] Semyon A. Grodsky, and James A. Carton
Department of Meteorology, University of Maryland, College Park, Maryland, USA

Michael J. McPhaden
NOAA/Pacific Marine Environmental Laboratory, Seattle, Washington, USA

Received 28 August 2003; revised 5 February 2004; accepted 16 February 2004; published 31 March 2004.

[1] Strong seasonal river discharge, precipitation, evaporation, and the confluence of different water masses all contribute to a complex surface salinity seasonal cycle in the western tropical Atlantic. This paper addresses the atmospheric and oceanic causes of the seasonal variability in mixed layer salinity based on direct observations. Primary data sets include up to 5 years (September 1997 to December 2002) of measurements from moored buoys of the Pilot Research Array in the Tropical Atlantic (PIRATA), ship-intake salinity observations, and near-surface drifting buoys. We analyze the mixed layer salt balance at four PIRATA mooring locations along 38°W (15°N, 12°N, 8°N, and 4°N). This region is strongly influenced by seasonally varying precipitation associated with the latitudinal migrations of the Intertropical Convergence Zone. Thus at all four locations we find that surface freshwater fluxes are a major contributor to the mixed layer salt balance. We also find that horizontal transport plays a key role at most locations. At 15°N a strong seasonal cycle of horizontal advection contributes to a semiannual cycle of local storage. At 12°N the balance is mostly controlled by local surface freshwater fluxes, with a minor contribution from meridional advection. The strongest seasonal cycle of precipitation occurs at 8°N, resulting in a strong seasonal cycle of local salt storage. At 4°N the dominant semiannual cycle of precipitation is reflected in the surface freshwater flux. However, zonal and meridional advection are also significant, resulting in a strong annual variation in the mixed layer salt storage at this location. Some implications of our results for tropical Atlantic climate variability are briefly discussed. *INDEX TERMS:* 4231 Oceanography: General: Equatorial oceanography; 4227 Oceanography: General: Diurnal, seasonal, and annual cycles; 4572 Oceanography: Physical: Upper ocean processes; *KEYWORDS:* salt budget, PIRATA buoy, tropical Atlantic

Citation: Foltz, G. R., S. A. Grodsky, J. A. Carton, and M. J. McPhaden (2004), Seasonal salt budget of the northwestern tropical Atlantic Ocean along 38°W, *J. Geophys. Res.*, *109*, C03052, doi:10.1029/2003JC002111.

1. Introduction

[2] Observational and modeling studies have shown that mixed layer salinity can dramatically affect currents and temperature in the tropics through the formation of barrier layers and through its effect on horizontal pressure gradients [*Lukas and Lindstrom*, 1991; *Carton*, 1991; *Roemmich et al.*, 1994; *Murtugudde and Busalacchi*, 1998; *Vialard and Delecluse*, 1998; *Pailler et al.*, 1999]. One of the regions where these effects are most likely to be important is the western tropical Atlantic, where salty subtropical water is overlaid by mixed layers that are strongly influenced by river discharge and precipitation. Studies of the salt budget of the mixed layer in the tropical Pacific and in the tropical Atlantic indicate that advective effects may be crucial as well [e.g., *Delcroix and Henin*, 1991; *Cronin and McPhaden*, 1998; *Delcroix and Picaut*, 1998; *Henin et al.*, 1998; *Johnson et al.*, 2002]. In this study we use in situ and satellite data to isolate these oceanic and atmospheric causes of the seasonal cycle of mixed layer salinity along the 38°W meridian.

[3] The annual mean surface freshwater flux reflects the mean position of tropical precipitation associated with the Intertropical Convergence Zone (ITCZ) and evaporation associated with the winds of the subtropical high-pressure systems. Away from the equator (south of 5°S and north of 10°N) evaporation dominates precipitation, while closer to the equator, precipitation dominates evaporation [*Schmitt et al.*, 1989]. Precipitation reaches an annual and zonal mean maximum of 20 cm mo^{-1} near 5°N, while

[1]Now at NOAA/Pacific Marine Environmental Laboratory, Seattle, Washington, USA.

Copyright 2004 by the American Geophysical Union.
0148-0227/04/2003JC002111$09.00

evaporation reaches a maximum of 15 cm mo^{-1} near 15°N [*Yoo and Carton*, 1990].

[4] Seasonal changes in the surface freshwater flux result mainly from latitudinal movements of tropical precipitation and, to a lesser extent, wind-driven evaporation, associated with the position of the ITCZ. In the northern tropics, evaporation peaks in boreal winter. In this season, the ITCZ is situated close to its southernmost latitude, with increasing northeast trade winds and decreasing relative humidity northward from the equator. In April, a band of high precipitation (>0.3 mm hr^{-1}) is situated west of 30°W between 5°S and 5°N, increasing westward toward the coast of South America. In boreal summer and fall, the ITCZ shifts to its northernmost latitude (10°N–12°N), resulting in higher relative humidity, lower wind speed, and less evaporation in the zone 5°N–10°N. Between the equator and 8°N the semiannual passage of the ITCZ results in a significant semiannual harmonic of the surface freshwater flux, with maxima in June and December and highest amplitude in the west [*da Silva et al.*, 1994].

[5] In addition to the surface freshwater flux, ocean circulation can affect mixed layer salinity along 38°W. Near-surface currents in the western tropical Atlantic are dominated by the westward South Equatorial Current south of 5°N and the eastward North Equatorial Countercurrent centered near 6°N, while sea surface salinity (SSS) increases from a minimum of ~35.5–36 psu at 5°N to 37 psu in the subtropics (Figure 1). The western current systems are subject to strong seasonal and eddy variability [*Richardson and Reverdin*, 1987] that affect SSS.

[6] Seasonal fluctuations of zonal currents and salinity gradients are strongest in the latitude band 4°N–8°N (Figure 2), in association with seasonal changes in the position of the ITCZ and the intensity of Amazon River discharge. In boreal winter a region of fresh water (<36 psu) extends northwestward along the coast of South America from the mouth of the Amazon to 15°N [*Dessier and Donguy*, 1994]. In boreal spring, as outflow from the Amazon increases, the fresh pool expands outward from the coast to 45°W and northward into the Caribbean [*Muller-Karger et al.*, 1995]. By late boreal summer and fall, coincident with the arrival of the ITCZ and the strengthening of the North Equatorial Countercurrent, a band of fresh water extends eastward across the basin between 4°N and 10°N. Associated with this fresh pool is a significant barrier layer that is maintained at the surface by eastward advection from the Amazon and at depth by southwestward advection of high-salinity water subducted in the subtropics [*Sprintall and Tomczak*, 1992; *Pailler et al.*, 1999].

[7] In a previous study by *Foltz et al.* [2003] of the seasonal mixed layer heat budget at the PIRATA mooring locations, it was found that the balance along 38°W was primarily between surface fluxes and local storage, with lesser contributions from horizontal advection and entrainment/mixing processes. For salinity, we anticipate that advection plays a much more important role due to the presence of strong horizontal gradients of salinity (Figure 2). To explore this possibility, we examine the seasonal mixed layer salinity budget at the same four PIRATA mooring locations along 38°W (Figure 1).

2. Data and Methods

[8] The derivation of the vertically integrated salt balance equation by *Delcroix and Henin* [1991] gives

$$h\frac{\partial S}{\partial t} = -h\left(\vec{v}\cdot\nabla S + \overline{\vec{v}'\nabla S'}\right) - (\Delta S)w_e - \nabla\cdot\int_{-h}^{0}\hat{\vec{v}}\hat{S}dz + (E-P)S + F_{-h}. \quad (1)$$

Here we have included the vertically integrated velocity/salinity covariance and vertical turbulent diffusion terms (third and fifth terms on the right) based on the derivation of an analogous heat balance equation [*Moisan and Niiler*, 1998]. Following *Stevenson and Niiler* [1983], entrainment velocity is written as

$$w_e = H\left(\frac{\partial h}{\partial t} + \nabla\cdot h\vec{v}\right). \quad (2)$$

The terms in equation (1) represent, from left to right, local salt storage, horizontal advection (separated into monthly mean and eddy terms), entrainment, vertical salinity/velocity covariance, surface freshwater flux, and turbulent diffusion at the base of the mixed layer. Entrainment velocity (equation (2)) is associated with a mass flux that crosses an isopycnal surface (H is the Heaviside unit function). Here h is the depth of the mixed layer, S and $\vec{v}$ are salinity and horizontal velocity, respectively, vertically and monthly averaged from the surface to a depth of $-h$, S' and $\vec{v}'$ are deviations from their monthly means (the overbar represents a monthly mean), $\hat{S}$ and $\hat{\vec{v}}$ represent deviations from the vertical average, $\Delta S = S - S_{-h}$, E is evaporation, and P is precipitation.

[9] Since in situ velocity measurements are not yet available at the moorings, we must neglect the vertical salinity/velocity covariance, horizontal eddy advection, and vertical turbulent diffusion terms in equation (1). On the basis of 10-day averaged salinity and velocity data of the SODA reanalysis [*Carton et al.*, 2000], we find that the vertical salinity/velocity covariance term at the buoy locations contributes no more than 0.8 mg m^{-2} s^{-1}, which is small compared to the dominant terms in equation (1). However, we anticipate that higher-frequency salinity and velocity fluctuations (on timescales < 10 days) may contribute significantly to this term. We also expect that high-frequency salinity and velocity fluctuations may result in significant horizontal and vertical turbulent diffusion, based on studies in the equatorial Pacific [e.g., *Hayes et al.*, 1991; *Lien et al.*, 2002].

[10] The PIRATA mooring array [*Servain et al.*, 1998] consists of 12 buoys. We focus on the four westernmost moorings (Figure 1) with record lengths of up to 5 years. Deployed in 1997 to study ocean-atmosphere interactions, these Next Generation Autonomous Temperature Line Acquisition System (ATLAS) buoys measure subsurface ocean temperature and salinity, rainfall, and surface air temperature, relative humidity, and wind velocity. Ocean temperature is

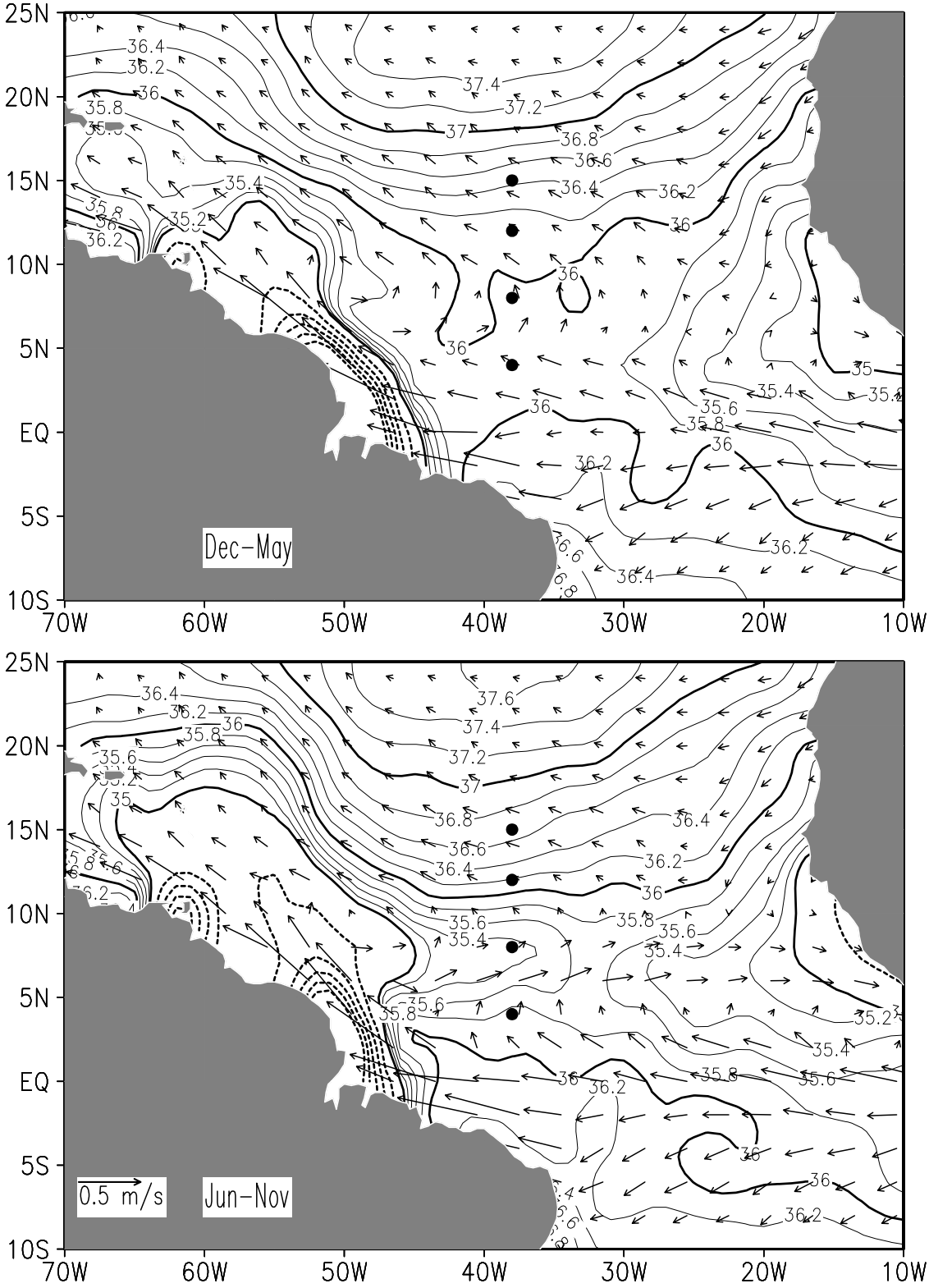

Figure 1. Locations of the PIRATA moored buoys used in this study (solid circles). Background contours and arrows are climatological winter-spring (averaged December–May) and summer-fall (averaged June–November) surface salinity from the *Dessier and Donguy* [1994] analysis of ship-intake data and near-surface ocean velocity from the *Grodsky and Carton* [2001] analysis of surface drifters. Bold contour lines represent 1 psu intervals.

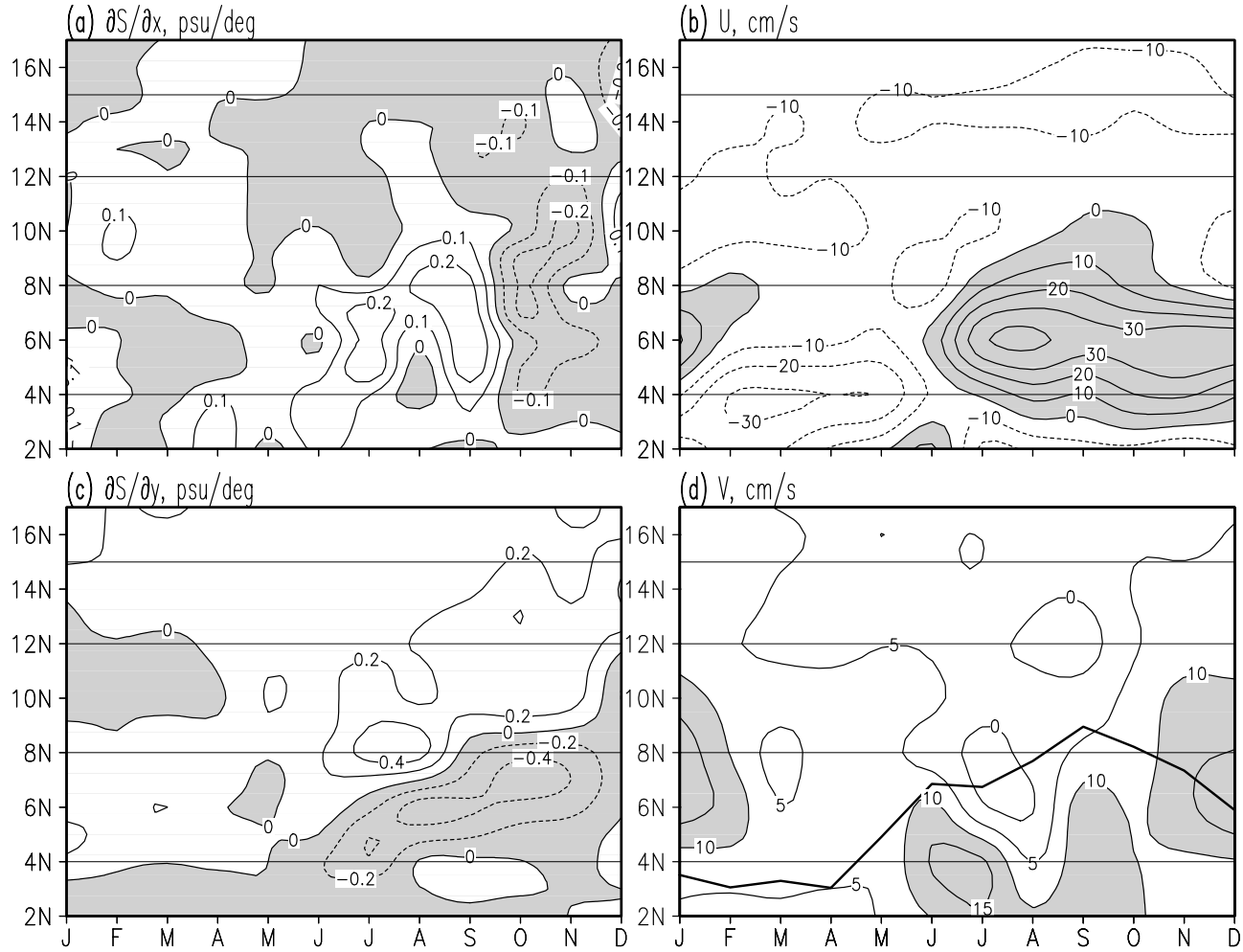

Figure 2. Seasonal variations of the sea surface salinity gradient, estimated from centered differences using the 1°lat × 1°lon × 1-month *Dessier and Donguy* [1994] climatology (left panels), and near-surface currents (right panels) at 38°W. The bold line in Figure 2d represents the position of the ITCZ (defined as the latitude of maximum QuikSCAT wind convergence).

measured at 11 depths between 1 and 500 m, with 20-m spacing in the upper 140 m, while salinity is measured only at 1, 20, 40, and 120 m. The 1-m temperature and salinity sensors provide bulk measures of sea surface temperature (SST) and SSS, respectively. Air temperature and relative humidity are measured at a height of 3 m above sea level, while rainfall and wind velocity are measured at 3.5 and 4 m, respectively. The sampling interval is 10 min for all variables except rainfall, which is sampled at 1-min intervals, then post-processed to 10-min values. The instrument accuracies are: water temperature within ±0.01°C, salinity within ±0.02 psu, wind speed ±0.3 m s^{-1} or 3% (whichever is greater), air temperature ±0.2°C, relative humidity ±3%, and rainfall ±0.4 mm hr^{-1} [*Freitag et al.*, 1994, 1999, 2001; *Serra et al.*, 2001, *Lake et al.*, 2003]. Here we use both 10-min and daily averaged data, which are transmitted to shore in real time via satellite by Service Argos, Inc.

[11] All 10-min PIRATA data used in this study (precipitation, air temperature, relative humidity, SST, and wind speed) have been analyzed by PMEL/NOAA for quality control purposes [*Freitag et al.*, 1999]. The quantity of 10-min quality-controlled subsurface salinity data is low, and thus we use daily averaged values based on real-time data streams, which are available with minimal quality control (H. P. Freitag, personal communication, 2003). We have carried out our own quality control for these data, which includes subjective removal of uncharacteristic high-frequency oscillations, removal of data with a significant bias (>1 psu) with respect to the mean of the remaining time series at that location, and elimination of data at any two depth levels for which the difference in salinity between the levels changes rapidly (indicating instrument drift).

[12] Precipitation is available directly from the moorings. In contrast, evaporation is estimated using the bulk parameterization, $E = \rho_a C_e W(q_s - q)$, where E is the evaporation rate, ρ_a is air density, C_e is the transfer coefficient, W is wind speed, q is the water vapor mixing ratio, and q_s is the interfacial water vapor mixing ratio, which is assumed to be proportional to the saturation water vapor mixing ratio. Comparisons of this algorithm, developed from the Coupled Ocean-Atmosphere Response Experiment (COARE) in the tropical west Pacific, to direct observations have revealed a bias of 2×10^{-3} mm hr^{-1} (COARE estimates are lower) [*Fairall et al.*, 1996]. We use 10-min measurements of air temperature, SST,

wind speed, and relative humidity to estimate evaporation and neglect both cool skin and warm layer effects (see *Foltz et al.* [2003] for an estimate of their magnitudes).

[13] Following the procedure of *Foltz et al.* [2003], we estimate the mixed layer depth as the depth at which density is 0.15 kg m^{-3} greater than the nighttime surface value (a 0.15 kg m^{-3} density step approximately corresponds to a 0.5°C temperature drop at SST of 28°C and SSS of 36 psu). Throughout much of the open upper ocean, density is controlled primarily by temperature. However, the western tropical Atlantic is affected by strong precipitation, river discharge, and persistent salinity fronts, all of which influence the mixed layer stratification. At the two southern locations (4°N and 8°N) the difference between the isothermal layer depth and the mixed layer depth (defining the barrier layer thickness) is greatest in boreal fall (Figures 3c and 3d). These thick barrier layers (reaching 40 m at 4°N) develop in response to the eastward extension of the low-salinity Amazon plume, driven by the seasonal strengthening of the North Equatorial Countercurrent in late summer and fall [*Carton*, 1991; *Pailler et al.*, 1999], and in response to ITCZ rainfall that develops in boreal summer through fall at 8°N and twice per year (boreal winter and late spring/early summer) at 4°N. The barrier layer widens to up to 20 m in boreal fall at 8°N. At 4°N a barrier layer persists throughout the year, thickening to ~30 m in early spring and up to ~40 m in early fall. At the two northern mooring locations (12°N and 15°N) the barrier layer widens in boreal winter, in phase with the strengthening of northward wind-driven transport of low-salinity waters over saltier subtropical waters to the north. Also shown in Figure 3 are climatological barrier layer thicknesses from the analysis of *Monterey and Levitus* [1997], which includes data from high-vertical-resolution CTD casts. These barrier layer thicknesses are similar to those derived from PIRATA data (though the *Monterey and Levitus* [1997] mixed layer depths are generally ~10 m shallower than the PIRATA mixed layer depths).

[14] To calculate horizontal salt advection and entrainment velocity, we first estimate the seasonal cycle of near-surface (~15 m) horizontal velocity following the procedure of *Grodsky and Carton* [2001] and *Foltz et al.* [2003]. This method uses quasi-Lagrangian drifter velocity, ship-drift velocity, and satellite-based sea level and wind stress. We anticipate that meridional velocity in the mixed layer is primarily the result of Ekman drift (since the trade winds are mainly zonal in the western basin) that decreases with increasing depth. We therefore apply a correction that assumes a linear decrease in meridional velocity from the observed value at 15 m to zero at $-h$, following *Foltz et al.* [2003]. Between the surface and 15 m, on the other hand, flow is assumed to be uniform since it is unclear how to reliably extrapolate the 15-m velocities to the surface. We have used the SODA ocean reanalysis of *Carton et al.* [2000] to estimate errors introduced by our assumptions. We find that the difference between meridional velocity vertically averaged in the mixed layer and that based on our assumed vertical profile is generally <3 cm s^{-1} on a monthly basis, leading to relative uncertainties ($\frac{V_{RMS}}{V_{STD}}$, where V_{RMS} is the monthly RMS difference between the two estimates and V_{STD} is the standard deviation of the SODA mixed layer meridional velocity) of 25–50%. Maximum monthly corrections to the salt balance (with respect to a constant vertical profile of meridional velocity) occur at 15°N during boreal winter (~1.7 mg m^{-2} s^{-1}), when the mixed layer is deep and the meridional salinity gradient is strong. Since we cannot estimate the vertical distribution of zonal velocity (we anticipate that it depends strongly on horizontal pressure gradients, which we cannot calculate), we have not applied a correction to zonal velocity estimates.

[15] We have considered two climatological data sets for estimating horizontal SSS gradients. The World Ocean Atlas [*Boyer et al.*, 2002] uses an objective analysis scheme that includes a five-point spatial smoother and a first-guess field consisting of the annual and zonal mean within the basin. In contrast, the *Dessier and Donguy* [1994] climatology, based on near-surface ship intake salinity measurements, includes only the Atlantic basin and uses the Kriging method without spatial smoothing. Both data sets are available on a 1°lat × 1°lon × 1-month grid. Agreement between the two data sets is best at the two northern locations (15°N and 12°N), with SSS, $\partial S/\partial x$, and $\partial S/\partial y$ RMS differences of <0.08 psu, 0.02 psu deg^{-1}, and 0.02 psu deg^{-1}, respectively, and maximum monthly differences of <0.4 psu, 0.2 psu deg^{-1}, and 0.2 psu deg^{-1}, respectively. At the two southern locations, differences are greatest during boreal summer and fall, with maximum monthly differences in SSS, $\partial S/\partial x$, and $\partial S/\partial y$ of up to 1.2 psu, 0.3 psu deg^{-1}, and 0.4 psu deg^{-1}, respectively. RMS differences in SSS and SSS gradients at these locations are as high as 0.11 psu and 0.04 psu deg^{-1}, respectively. In this study we use monthly SSS gradients from the *Dessier and Donguy* [1994] climatology, along with the horizontal velocity estimates discussed above, to estimate horizontal salt advection.

[16] We use the divergence of the velocity estimates, as well as estimates of the time derivative of mixed layer depth (MLD) based on PIRATA subsurface temperature and salinity, to calculate w_e (see equation (2)). Horizontal gradients of h are estimated from the 2°lat × 5°lon × 1-month isothermal layer depth (ILD) climatology of *White* [1995]. Substitution of *Monterey and Levitus* [1997] MLD gradients, which are based on the 1994 World Ocean Atlas, reduces entrainment by at most 0.2 mg m^{-2} s^{-1} on a monthly basis at 12°N, 8°N, and 4°N and up to 0.8 mg m^{-2} s^{-1} during boreal winter at 15°N. We anticipate that this reduction is due to a combination of spatial smoothing by *Monterey and Levitus* [1997] and the fact that, in general, MLD < ILD. We therefore scale the $\vec{v} \cdot \nabla h$ term in equation (2) by $\frac{\mathrm{MLD}_{\mathrm{PIRATA}}}{\mathrm{ILD}_{\mathrm{White(1995)}}}$.

[17] In order to smooth high-frequency variability that our data cannot accurately reproduce, we fit each term in equation (1) to annual and semiannual harmonics using least squares (Fourier) analysis (see Appendix A for further details). This fitting procedure allows us to produce a consistent analysis of the gappy buoy series. It typically accounts for 40–70% of the total variance, which includes a range of energetic frequencies between intraseasonal and interannual. Although the data span a maximum of 5 years, they reveal a discernible seasonal cycle for most surface variables, illustrated for 8°N in Figure 4.

3. Results

[18] In this section we examine the balance of terms in equation (1) at four PIRATA buoy locations (Figure 1). We

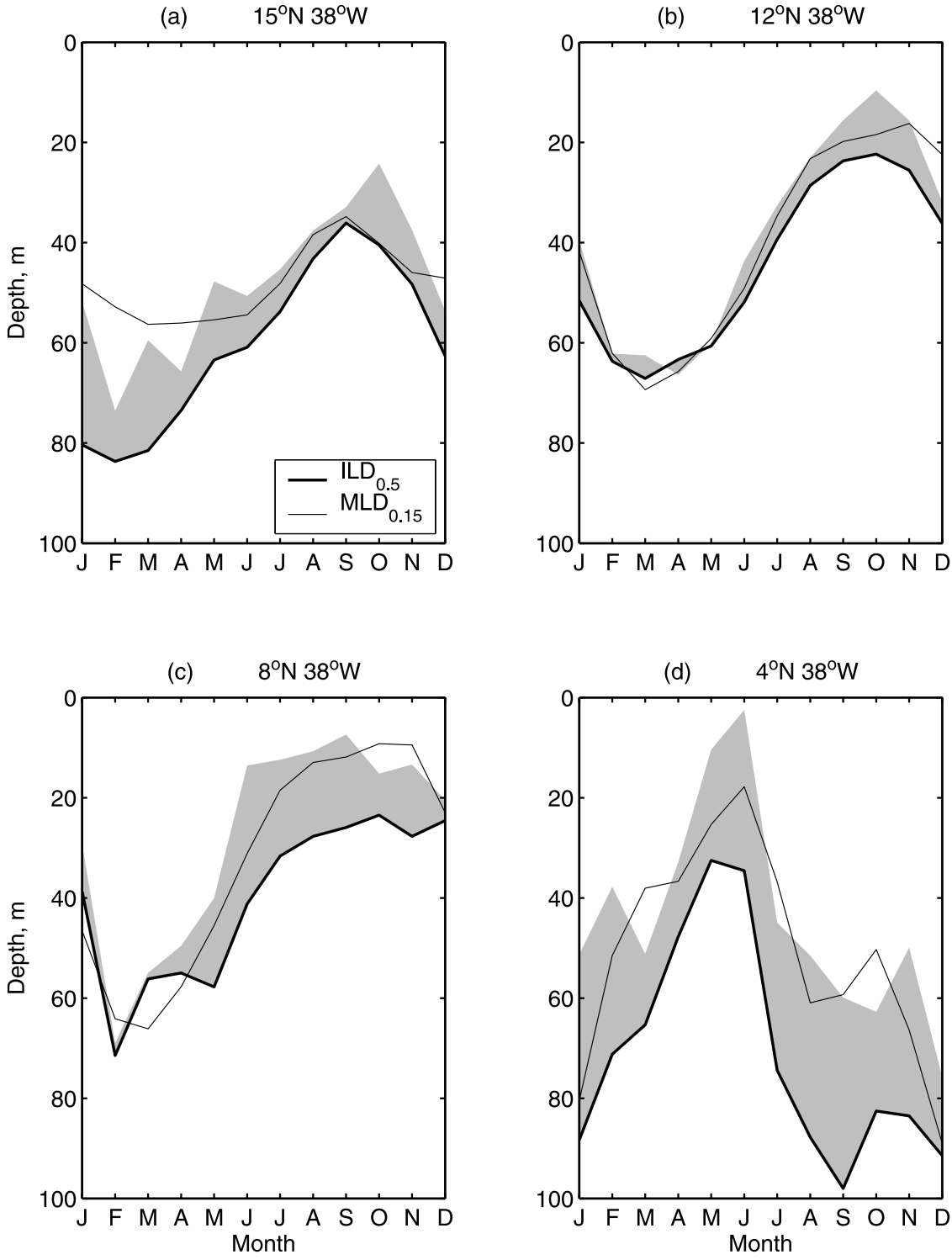

Figure 3. Comparison of the isothermal mixed layer depth based on a 0.5°C criterion, $ILD_{0.5}$, and the mixed layer depth based on a 0.15 kg m^{-3} density criterion, $MLD_{0.15}$. The difference between the two is the barrier layer thickness. Shading indicates the barrier layer thickness based on the $ILD_{0.5}$ and $MLD_{0.125}$ estimates of *Monterey and Levitus* [1997] and referenced to PIRATA $ILD_{0.5}$ values. The difference between $MLD_{0.15}$ and $MLD_{0.125}$ is generally 1–2 m.

begin by considering two locations situated north of the ITCZ throughout the year, and then examine the two southernmost locations, which bracket the mean latitudinal position of the ITCZ (Figure 2d).

3.1. 15°N and 12°N

[19] At these sites, surface fluxes contribute significantly to seasonal salt storage (Figures 5 and 6). The surface freshwater flux is mostly annual and is connected to the

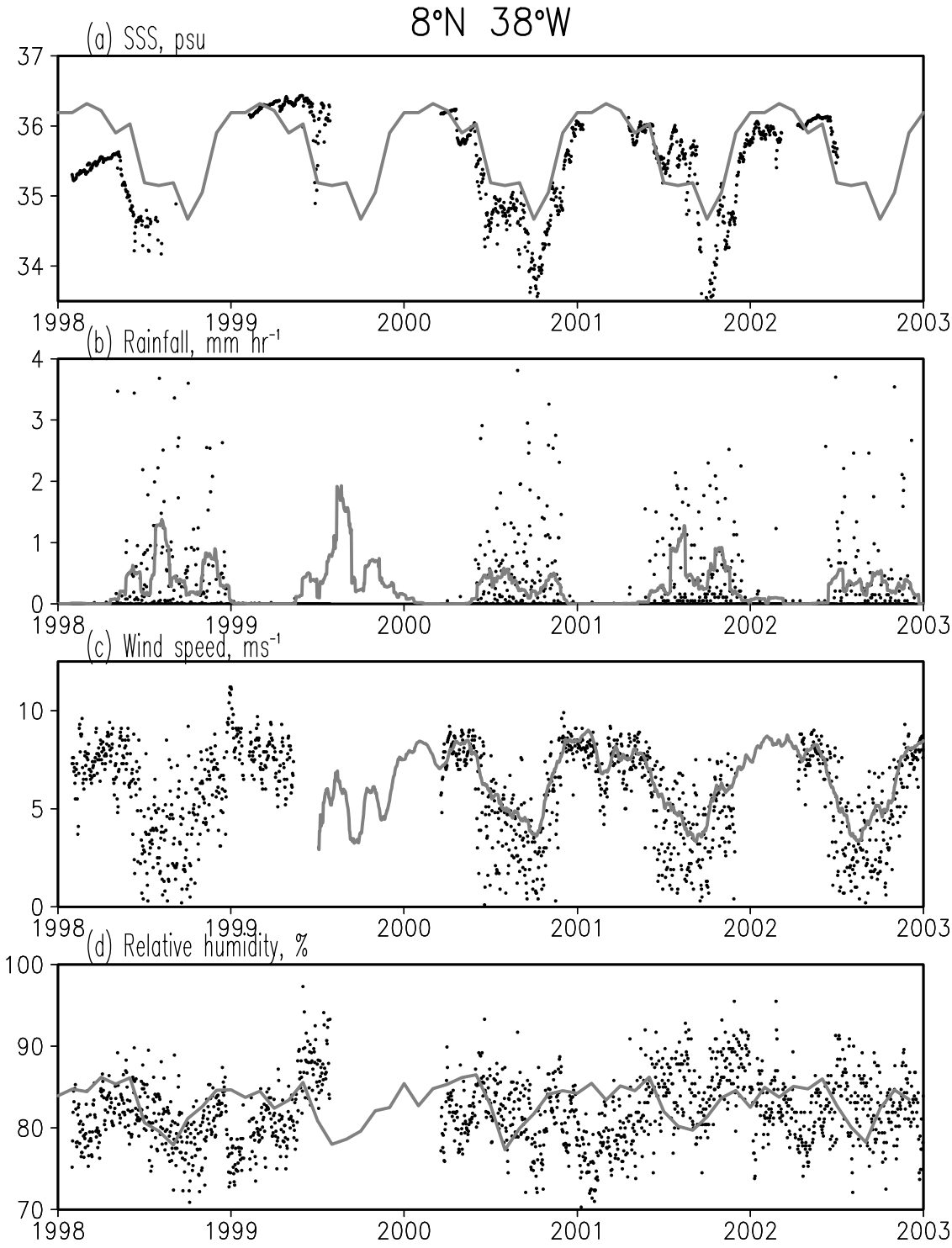

Figure 4. Daily PIRATA near-surface atmospheric and oceanic measurements at 8°N, 38°W during 1998–2002. For comparison, solid shaded lines represent climatological monthly mean surface salinity (from the *Dessier and Donguy* [1994] analysis), TRMM Microwave Imager/Precipitation Radar rainfall, QuikSCAT near-surface wind speed (recalculated to a height of 4 m), and NCEP/NCAR Reanalysis relative humidity.

seasonal meridional march of the ITCZ. Rainfall is significant during August–November, when the ITCZ is near its northernmost position (Figure 2d shows the ITCZ position), while evaporation is at a minimum during August–September. As a result, surface salinity decreases at both locations during late boreal summer and early fall. In boreal winter the ITCZ shifts southward, resulting in decreased rainfall at 12°N and 15°N. The southward ITCZ shift also results in a strengthening of the northeast trade winds and a decrease in relative humidity that, in turn, lead to high rates of evapo-

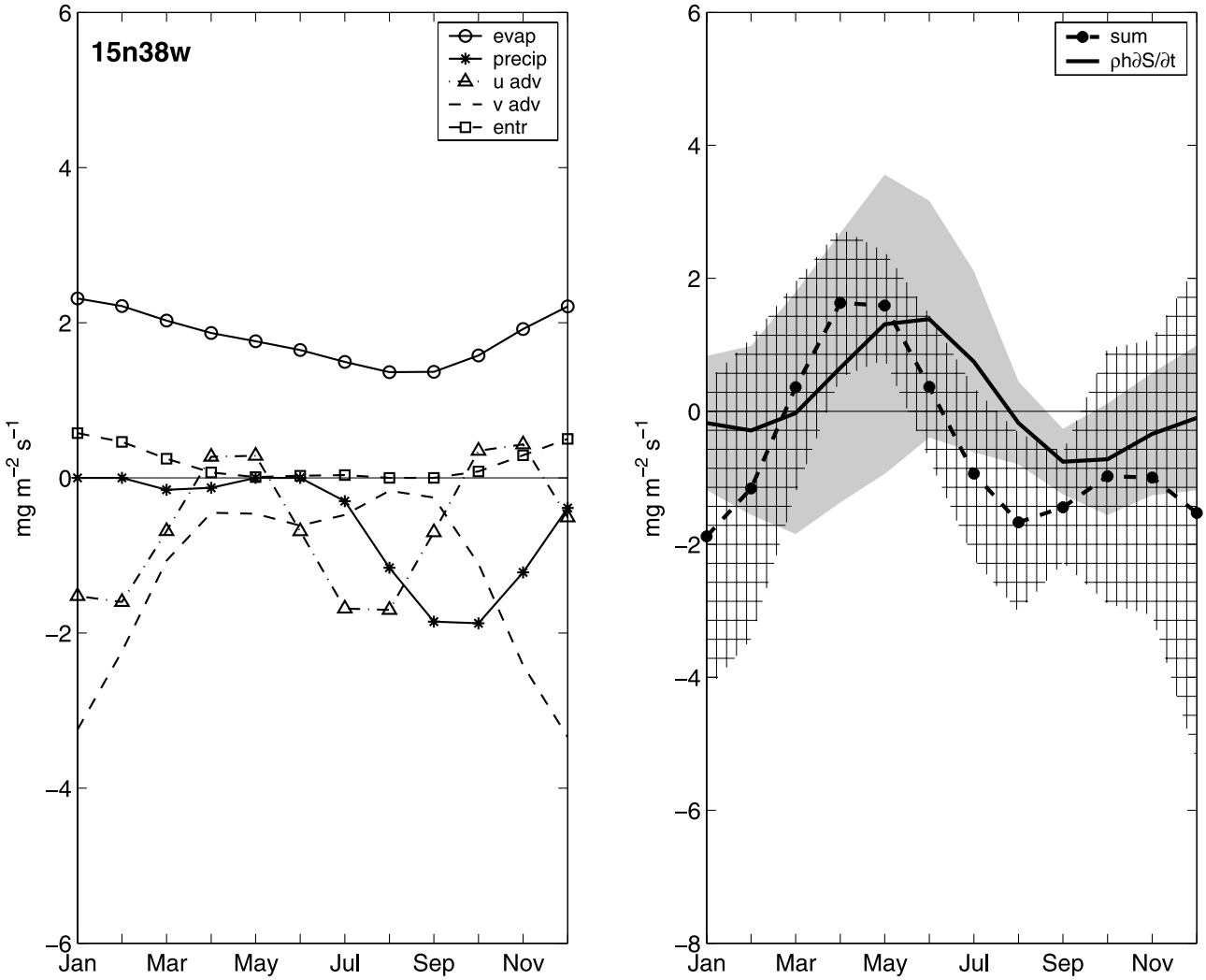

Figure 5. The mixed layer salt balance at 15°N, 38°W. Left panel shows individual contributions to the salt balance equation (1) in the form of evaporation, precipitation, entrainment, and mean zonal and meridional salt advection. Lines in left panel show least squares fits of annual mean plus annual and semiannual harmonics to monthly data. Lines in right panel show the sum of the terms in the left panel and the mixed layer salt storage rate. Shading and cross-hatching in right panel indicate error estimates (see Appendix A) for the salt storage rate and the sum of terms, respectively.

ration. These changes in the surface flux cause surface salinity to increase at 12°N. At 15°N, freshening due to zonal and meridional advection exceeds the effects of evaporation, leading to a weak freshening in boreal winter.

[20] At 12°N, surface fluxes are primarily responsible for the seasonal cycle of mixed layer salinity, while ocean circulation plays a lesser role. The zonal gradient of salinity is weak, resulting in a very weak seasonal cycle of zonal advection. Interestingly, there are seasonal variations in the meridional salinity gradient that reflect the meridional march of the ITCZ. Indeed, the meridional gradient at 12°N increases in boreal summer and fall (Figure 2c). However, the mixed layer is shallow (Figure 3b) and the meridional currents are weak during this season, reducing the contribution of horizontal advection to the seasonal salinity budget.

[21] In contrast, at 15°N, horizontal transport is an important factor in the annual and semiannual signal of the salt budget. Meridional velocity reaches a maximum during boreal winter (Figure 2d), when the northeasterly trade winds and resultant northward Ekman drift are strong. The northward salinity gradient at 15°N is also strongest during boreal winter, when evaporation rates are high to the north and rainfall is abundant to the south (Figure 2c). As a result, and in combination with a deep mixed layer (Figure 3a), meridional advection provides a significant source of freshening at 15°N in boreal winter (Figure 5). This is in contrast to the situation at 12°N, where the meridional salinity gradient is slightly negative during winter, resulting in a much weaker seasonal cycle of meridional advection (Figure 6).

[22] Zonal advection is weaker than meridional advection at 15°N because of the weaker zonal gradient of salinity. This weak zonal salinity gradient is negative (i.e., higher salinity in the west) throughout most of the year, becoming strongest during late boreal summer, when evaporation

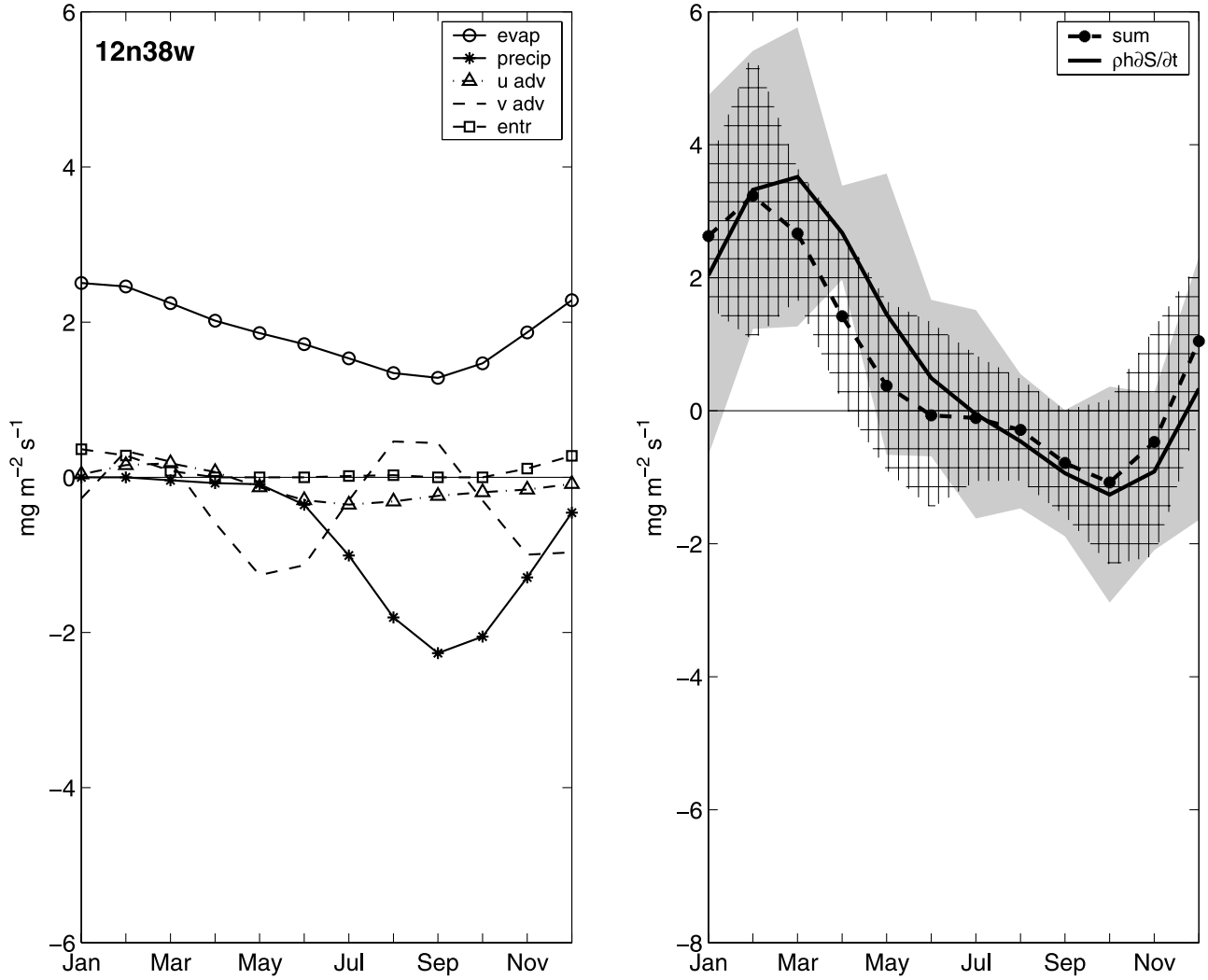

Figure 6. As in Figure 5, but for 12°N, 38°W.

reaches a minimum to the east, and boreal winter, when evaporation is at a maximum to the west. As a result, the westward North Equatorial Current provides a source of freshening that varies semiannually. A decrease in negative zonal salt transport partially accounts for the positive rate of storage in boreal spring (Figure 5). Entrainment at these latitudes is small and is associated with a deepening mixed layer in boreal fall and winter that acts to increase mixed layer salinity.

3.2. 8°N and 4°N

[23] We next consider two locations within the latitudinal range of the ITCZ (8°N and 4°N; Figures 7 and 8, respectively). As at 15°N and 12°N, rainfall at 8°N is dominated by the annual harmonic, with a maximum in early fall, when the ITCZ is farthest north. At 4°N, rainfall is primarily semiannual, associated with the double passage of the ITCZ in May–June and in December.

[24] Seasonal variations of evaporation at 4°N are weaker than those to the north (12°N and 15°N) due to weaker variations of wind speed and relative humidity at 4°N. At 8°N, evaporation is larger than at 12°N and 15°N during boreal summer and fall despite the fact that 8°N lies within the low mean wind regime of the ITCZ during these seasons (Figure 2d). Although the differences in evaporation at these locations are smaller than our uncertainty estimates of ~0.5 mg m^{-2} s^{-1}, we note that the strong evaporation at 8°N during July–October may be due in part to very warm SST. During boreal summer and fall, SST at 8°N remains at least 1°C warmer than at 12°N and 15°N, reaching up to 30°C during September. We have also found significant mesoscale enhancement of evaporation at 8°N, caused by fluctuations of wind velocity on timescales of less than 1 month (*Esbensen and McPhaden* [1996] report similar results in the tropical Pacific). The difference between monthly evaporation (latent heat loss) calculated with 10-min scalar-averaged wind speed and that calculated with monthly vector-averaged wind speed reaches 0.8 mg m^{-2} s^{-1} (60 W m^{-2}) during July–September at 8°N and is nearly zero during November–May. There is a similar seasonal cycle of mesoscale enhancement at 12°N, with an amplitude that is about half that at 8°N, while at 15°N, mesoscale enhancement is nearly zero throughout the year.

[25] Although precipitation is the most important factor affecting seasonal variations of mixed layer salinity at 8°N and 4°N, horizontal transport is also important. At 8°N the

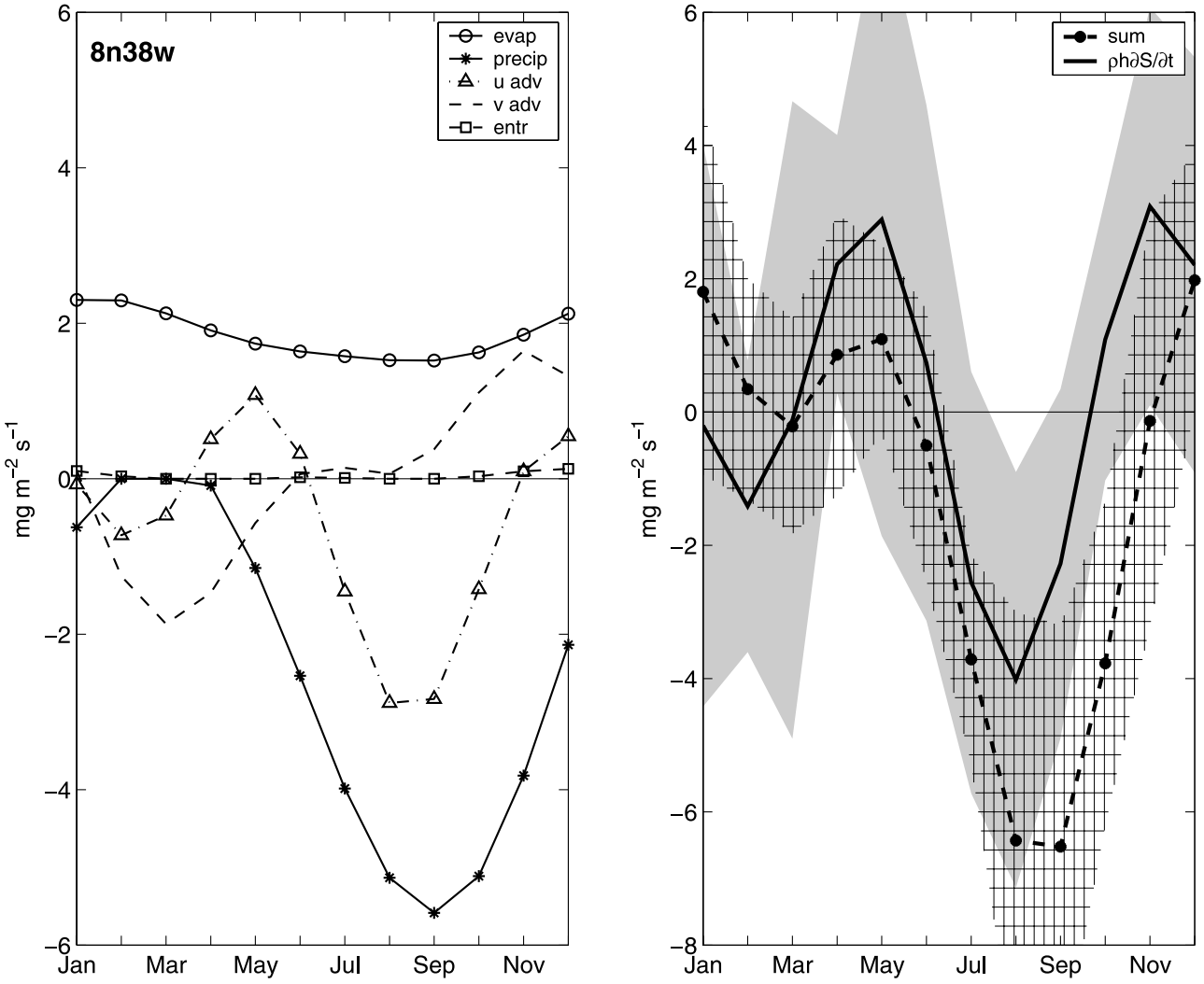

Figure 7. As in Figure 5, but for 8°N, 38°W.

meridional gradient of salt is positive January through August, with a maximum in July (Figure 2c). In fall the gradient becomes negative in response to the presence of ITCZ rainfall to the north (Figure 2d for the ITCZ latitude). As a result, meridional advection by the prevailing northward currents freshens the mixed layer during January–May, but increases mixed layer salinity in the fall (Figure 7). At 4°N the meridional gradient of salinity is weakly positive or negative throughout the year (Figure 2c), reaching a minimum in boreal summer when both the ITCZ and the Amazon freshwater plume are situated to the north. In this season, meridional velocity also reaches a maximum at 4°N (Figure 2d), due mainly to Ekman drift, resulting in significant northward salt advection.

[26] Zonal advection also contributes significantly at 8°N and 4°N (Figures 7 and 8). At 8°N, zonal currents are strongest during July–October, when the eastward North Equatorial Countercurrent reaches a maximum (Figure 2b). During this time the zonal gradient of salinity is generally positive (Figure 2a), due to eastward advection of low-salinity Amazon water, resulting in freshening of ~3 mg m^{-2} s^{-1} (Figure 7). At 4°N (Figure 2b), zonal currents on average are westward during the first half of the year (due to the South Equatorial Current) and eastward during the latter half (due to the North Equatorial Countercurrent). The zonal gradient of salinity also varies seasonally, leading to a semiannual variation in zonal transport (Figure 8). Entrainment at these locations is generally weak.

[27] Finally, we note the presence of substantial discrepancies in the salinity balance at 8°N, indicating that some terms may have been improperly represented or were neglected. We anticipate that horizontal eddy advection, turbulent exchange across the bottom of the mixed layer (the mixed layer is very shallow during the second half of the year at 8°N; Figure 3c), and the vertical salinity/velocity covariance term may account for at least part of the discrepancies present during late boreal summer and fall.

4. Summary

[28] This paper attempts to provide a systematic analysis of the salt budget for the mixed layer of the western tropical Atlantic, a region of complex processes, including strong precipitation, evaporation, river discharge, and fluctuating mixed layer depths. Our analysis exploits the availability of measurements from four PIRATA moorings and other in

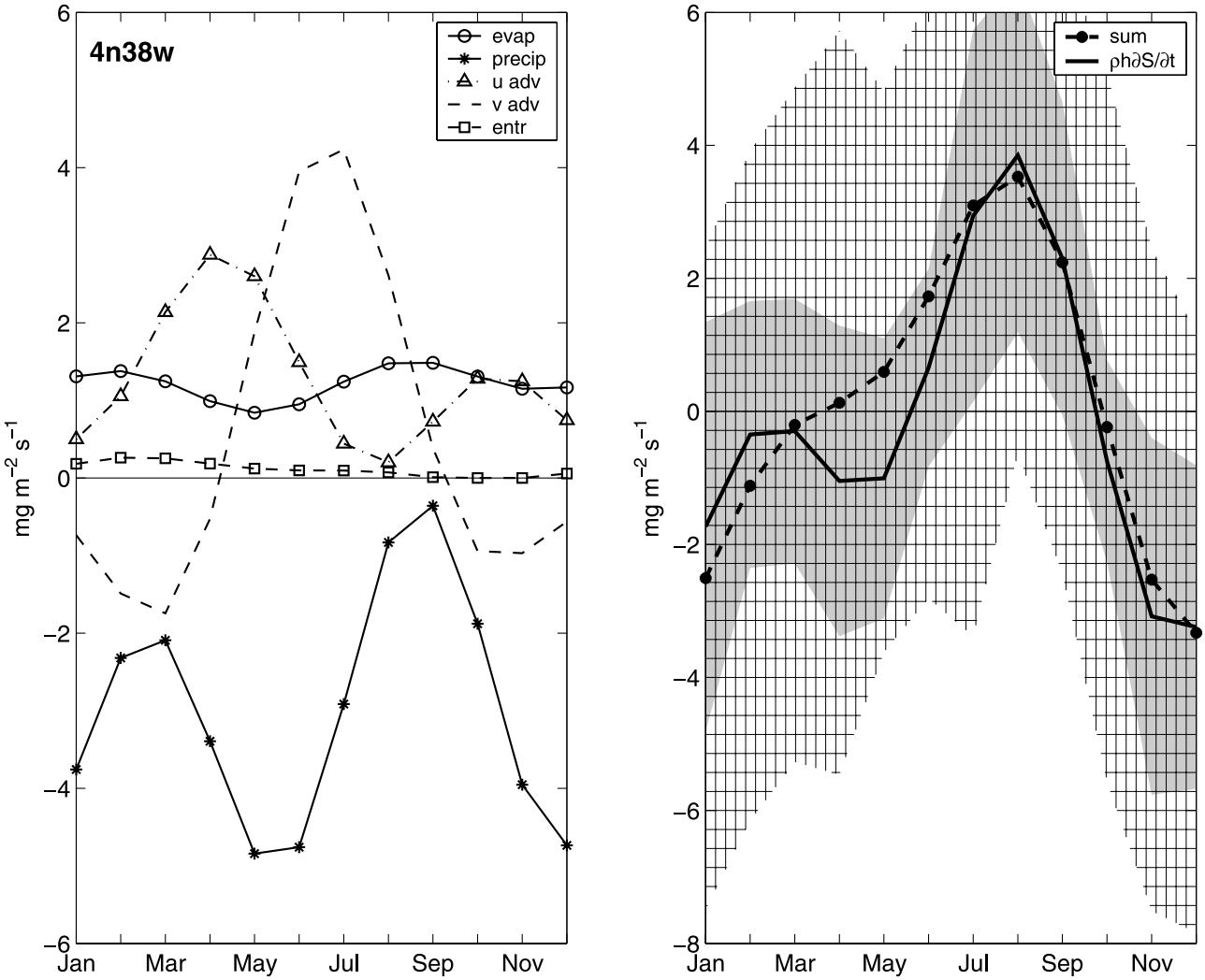

Figure 8. As in Figure 5, but for 4°N, 38°W.

situ data. It follows the spirit of a similar study by *Cronin and McPhaden* [1998] in the western equatorial Pacific. We have found that horizontal transport is an important component of the mixed layer salt balance in the northwestern tropical Atlantic, resulting from strong horizontal salinity gradients in the presence of relatively weak ocean currents ($\sim$10 cm s^{-1}). Our main results are as follows:

[29] • At 15°N, surface fluxes (evaporation and precipitation) and horizontal transport contribute significantly to seasonal changes of mixed layer salinity. The negative tendency of salinity storage in boreal fall is due to the presence of the ITCZ, which provides strong precipitation and weak evaporation. Zonal salt transport by the westward currents varies semiannually, reflecting changes in the zonal gradient of salinity. This component of transport accounts in part for the local maxima in the salinity storage rate in both boreal spring and late fall. Both components of transport account for the freshening tendency in boreal winter.

[30] • At 12°N, surface fluxes are most important in balancing local storage, with horizontal transport playing a lesser role. The reduction in zonal transport at this latitude (in comparison to that at 15°N) is due to weaker westward currents, while the reduction in meridional transport results from a decrease in the meridional salinity gradient.

[31] • At 8°N, both surface fluxes and horizontal transport are important. The freshening effects of precipitation and zonal advection are most important during boreal summer and fall. Freshening due to eastward currents in boreal summer and fall and the positive salinity tendency due to northwestward Ekman flow during fall are both enhanced by the eastward transport of waters partly diluted by Amazon discharge.

[32] • The mixed layer salt balance at 4°N includes significant contributions from semiannually varying precipitation and horizontal advection, which combine to create a strong annual cycle of local storage. Seasonal changes in evaporation are less significant at this location. Meridional advection provides a positive salt flux in boreal summer, reflecting a strengthening of both the southward salinity gradient and the northward wind-driven currents associated with the seasonal northward shift of the ITCZ. Westward transport by the South Equatorial Current in the first half of the year and eastward transport by the North Equatorial Countercurrent in the second half result in a strong annual cycle of zonal salinity advection, with peak eastward transport in boreal spring.

[33] Strong seasonal variations of horizontal salt transport are associated with the meridional movement of the ITCZ as

well as with seasonal changes in the magnitude of freshwater discharge from the Amazon River and the direction in which it is carried by oceanic currents. Thus surface fluxes and river discharge indirectly affect the salt budget through the formation of strong horizontal salinity gradients in the presence of horizontal currents. These results are in striking contrast to the mixed layer heat balance along 38°W, in which horizontal advection makes minimal contributions [*Foltz et al.*, 2003] due to weak surface temperature gradients. One important implication of our results is that ocean circulation anomalies in the western tropical Atlantic may result in strong anomalies of salinity, and hence sea level [e.g., *Segschneider et al.*, 2000]. Thus it is likely that accurate SSS fields, as well as horizontal velocity fields, will be required to fully understand and predict climate variability in this region.

[34] There are large uncertainties in our estimates of horizontal salt advection due to a lack of direct velocity measurements as well as a lack of salinity surveys. These uncertainties are largest at 8°N, where horizontal and vertical salinity gradients are strong. We have neglected several terms in the salt balance equation (horizontal eddy diffusion and vertical salinity/velocity covariance) due to a lack of in situ velocity data. We have also neglected vertical turbulent diffusion because we have no reliable way to estimate it. As a result, our study is inconclusive regarding these terms. There are also uncertainties in the estimates of the seasonal cycle due to the relatively short mooring records. Despite these uncertainties, it is clear that horizontal advection is an important component of the mixed layer salt balance. In contrast, entrainment plays a more limited role. To improve our knowledge of the seasonal salinity budget, it will be necessary to improve our estimates of horizontal salt transport. The addition to the PIRATA buoys of current meters and more salinity sensors in the upper 120 m, as well as satellite-based estimates of surface salinity, would all lead to better estimates of seasonal salt transport within the mixed layer. Though subject to considerable uncertainties because of data limitations, our results nonetheless provide a basis for evaluating interannual and decadal variability, which are both linked to perturbations of the seasonal cycle.

Appendix A: Harmonic Fitting and Error Estimates

[35] Terms in the seasonal salt budget (see equation (1)) are estimated in the following way. Let the matrix **Y** contain the monthly mean state observations, while **A** is the annual mean plus annual and semiannual harmonics filter, and **V** is a diagonal matrix containing the observational error covariance estimates. The filtered state estimate, **X**, is obtained by minimizing the cost function

$$J = (\mathbf{Y} - \mathbf{AX})^{T}\mathbf{V}^{-1}(\mathbf{Y} - \mathbf{AX}). \quad (3)$$

The total error, ϵ, associated with each term in equation (1) is estimated assuming the error associated with representing the observations by the annual mean plus two harmonics, ϵ_{fit}, and the error associated with estimating those harmonics from our limited data set, ϵ^2_{obs} = diag(**V**), are independent: $\epsilon = \sqrt{\left(\epsilon^2_{obs} + \epsilon^2_{fit}\right)}$. Here ϵ_{obs} is assessed as the standard deviations from the mean of all daily estimates for each climatological month. The total errors shown for the sums of terms in Figures 5–8 are estimated as the square root of the sum of the squared errors, ϵ, of the terms on the right of equation (1) on the assumption that the errors are uncorrelated between the terms. Typical values of ϵ_{fit} and ϵ_{obs} are 0.5–2 mg m^{-2} s^{-1} and 1–3 mg m^{-2} s^{-1}, respectively, with ϵ_{obs} generally exceeding ϵ_{fit} on a monthly basis. Note that we have also assumed that the accuracy of the PIRATA sensors is much higher than the "noise" introduced by fluctuations due to high-frequency processes that are not resolved by our analysis.

[36] **Acknowledgments.** This work was supported by NOAA's Office of Oceanic and Atmospheric Research and Office of Global Programs. The authors gratefully acknowledge the support provided by the National Science Foundation. We are grateful to the Drifter DAC of the GOOS Center at NOAA/AOML for providing the drifter data set. Alain Dessier has made the SSS ship-intake archive accessible via http://www.brest.ird.fr/sss/clim_atl.html. QuikSCAT wind velocity has been obtained from the NASA/NOAA sponsored system Seaflux at JPL through the courtesy of W. Timothy Liu and Wenqing Tang.

References

Boyer, T. P., C. Stephens, J. I. Antonov, M. E. Conkright, R. A. Locarnini, T. D. O'Brien, and H. E. Garcia (2002), *World Ocean Atlas 2001*, vol. 2, *Salinity*, edited by S. Levitus, *NOAA Atlas NESDIS 50*, 165 pp., Natl. Oceanic and Atmos. Admin., Silver Spring, Md.

Carton, J. A. (1991), Effect of seasonal surface freshwater flux on sea surface temperature in the tropical Atlantic Ocean, *J. Geophys. Res.*, *96*, 12,593–12,598.

Carton, J. A., G. Chepurin, X. H. Cao, and B. Giese (2000), A simple ocean data assimilation analysis of the global upper ocean 1950–95: I. Methodology, *J. Phys. Oceanogr.*, *30*, 294–309.

Cronin, M. F., and M. J. McPhaden (1998), Upper ocean salinity balance in the western equatorial Pacific, *J. Geophys. Res.*, *103*, 27,567–27,588.

da Silva, A., A. C. Young, and S. Levitus (1994), *Atlas of Surface Marine Data 1994*, vol. I, *Algorithms and Procedures*, *NOAA Atlas NESDIS 6*, Natl. Oceanic and Atmos. Admin., Silver Spring, Md.

Delcroix, T., and C. Henin (1991), Seasonal and interannual variations of sea surface salinity in the tropical Pacific Ocean, *J. Geophys. Res.*, *96*, 22,135–22,150.

Delcroix, T., and J. Picaut (1998), Zonal displacement of the western equatorial Pacific "fresh pool," *J. Geophys. Res.*, *103*, 1087–1098.

Dessier, A., and J. R. Donguy (1994), The sea surface salinity in the tropical Atlantic between 10°S and 30°N-Seasonal and interannual variations (1977–1989), *Deep Sea Res., Part I*, *41*, 81–100.

Esbensen, S. K., and M. J. McPhaden (1996), Enhancement of tropical ocean evaporation and sensible heat flux by atmospheric mesoscale systems, *J. Clim.*, *9*, 2307–2325.

Fairall, C. W., E. F. Bradley, D. P. Rogers, J. B. Edson, and G. S. Young (1996), Bulk parameterization of air-sea fluxes for TOGA COARE, *J. Geophys. Res.*, *101*, 3747–3764.

Foltz, G. R., S. A. Grodsky, J. A. Carton, and M. J. McPhaden (2003), Seasonal mixed layer heat budget of the tropical Atlantic Ocean, *J. Geophys. Res.*, *108*, 3146, doi:10.1029/2002JC001584.

Freitag, H. P., Y. Feng, L. J. Mangum, M. J. McPhaden, J. Neander, and L. D. Stratton (1994), Calibration procedures and instrumental accuracy estimates of TAO temperature, relative humidity, and radiation measurements, *NOAA Tech. Memo. ERL PMEL-104*, 32 pp., Natl. Oceanic and Atmos. Admin., Silver Spring, Md.

Freitag, H. P., M. E. McCarty, C. Nosse, R. Lukas, M. J. McPhaden, and M. F. Cronin (1999), COARE Seacat data: Calibrations and quality control procedures, *NOAA Tech. Memo. ERL PMEL-115*, 89 pp., Natl. Oceanic and Atmos. Admin., Silver Spring, Md.

Freitag, H. P., M. O'Haleck, G. C. Thomas, and M. J. McPhaden (2001), Calibration procedures and instrumental accuracies for ATLAS wind measurements, *NOAA Tech. Memo. OAR PMEL-119*, 20 pp., Natl. Oceanic and Atmos. Admin., Silver Spring, Md.

Grodsky, S. A., and J. A. Carton (2001), Intense surface currents in the tropical Pacific during 1996–1998, *J. Geophys. Res.*, *106*, 16,673–16,684.

Hayes, S. P., P. Chang, and M. J. McPhaden (1991), Variability of the sea surface temperature in the eastern equatorial Pacific during 1986–1988, *J. Geophys. Res.*, *96*, 10,553–10,566.

Henin, C., Y. du Penhoat, and M. Ioualalen (1998), Observations of sea surface salinity in the western Pacific fresh pool: Large-scale changes in 1992–1995, *J. Geophys. Res.*, *103*, 7523–7536.

Johnson, E. S., G. S. E. Lagerloef, J. T. Gunn, and F. Bonjean (2002), Salinity advection in the tropical oceans compared to atmospheric forcing: A trial balance, *J. Geophys. Res.*, *107*, 8014, doi:10.1029/2001JC001122.

Lake, B. J., S. M. Noor, H. P. Freitag, and M. J. McPhaden (2003), Calibration procedures and instrumental accuracy estimates for ATLAS air temperature and relative humidity measurements, *NOAA Tech. Memo.*, in press.

Lien, R.-C., E. A. D'Asaro, and M. J. McPhaden (2002), Internal waves and turbulence in the upper central equatorial Pacific: Lagrangian and Eulerian observations, *J. Phys. Oceanogr.*, *32*, 2619–2639.

Lukas, R., and E. Lindstrom (1991), The mixed layer of the western equatorial Pacific Ocean, *J. Geophys. Res.*, *96*, Suppl., 3343–3357.

Moisan, J. R., and P. P. Niiler (1998), The seasonal heat budget of the North Pacific: Net heat flux and heat storage rates (1950–1990), *J. Phys. Oceanogr.*, *28*, 401–421.

Monterey, G. I., and S. Levitus (1997), *Seasonal Variability of Mixed Layer Depth for the World Ocean*, *NOAA NESDIS Atlas 14*, 5 pp., 87 plates, Natl. Oceanic and Atmos. Admin., Silver Spring, Md.

Muller-Karger, F. E., P. L. Richardson, and D. McGillicuddy (1995), On the offshore dispersal of the Amazon's plume in the North Atlantic: Comments on the paper by A. Longhurst, ''Seasonal cooling and blooming in tropical oceans'', *Deep Sea Res., Part I*, *42*, 2127–2137.

Murtugudde, R., and A. J. Busalacchi (1998), Salinity effects in a tropical ocean model, *J. Geophys. Res.*, *103*, 3283–3300.

Pailler, K., B. Bourles, and Y. Gouriou (1999), The barrier layer in the western tropical Atlantic Ocean, *Geophys. Res. Lett.*, *26*, 2069–2072.

Richardson, P. L., and G. Reverdin (1987), Seasonal cycle of velocity in the Atlantic North Equatorial Countercurrent as measured by surface drifters, current meters, and ship drifts, *J. Geophys. Res.*, *92*, 3691–3708.

Roemmich, D., M. Morris, W. R. Young, and J. R. Donguy (1994), Fresh equatorial jets, *J. Phys. Oceanogr.*, *24*, 540–558.

Schmitt, R. W., P. S. Bogden, and C. E. Dorman (1989), Evaporation minus presipitation and density fluxes for the North Atlantic, *J. Phys. Oceanogr.*, *19*, 1208–1221.

Segschneider, J., M. Balmaseda, and D. L. T. Anderson (2000), Anomalous temperature and salinity variations in the tropical Atlantic: Possible causes and implications for the use of altimeter data, *Geophys. Res. Lett.*, *27*, 2281–2284.

Serra, Y. L., P. A'Hearn, H. P. Freitag, and M. J. McPhaden (2001), ATLAS self-siphoning rain gauge error estimates, *J. Atmos. Oceanic Technol.*, *18*, 1989–2002.

Servain, J., A. J. Busalacchi, M. J. McPhaden, A. D. Moura, G. Reverdin, M. Vianna, and S. E. Zebiak (1998), A pilot research moored array in the tropical Atlantic (PIRATA), *Bull. Am. Meteorol. Soc.*, *79*, 2019–2031.

Sprintall, J., and M. Tomczak (1992), Evidence of the barrier layer in the surface layer of the tropics, *J. Geophys. Res.*, *97*, 7305–7316.

Stevenson, J. W., and P. P. Niiler (1983), Upper ocean heat budget during the Hawaii-to-Tahiti shuttle experiment, *J. Phys. Oceanogr.*, *13*, 1894–1907.

Vialard, J., and P. Delecluse (1998), An OGCM study for the TOGA decade: I. Role of salinity in the physics of the western Pacific fresh pool, *J. Phys. Oceanogr.*, *28*, 1071–1088.

White, W. B. (1995), Design of a global observing system for gyre-scale upper ocean temperature variability, *Prog. Oceanogr.*, *36*, 169–217.

Yoo, J.-M., and J. A. Carton (1990), Annual and interannual variation of the freshwater budget in the tropical Atlantic Ocean and the Caribbean Sea, *J. Phys. Oceanogr.*, *20*, 831–845.

J. A. Carton and S. A. Grodsky, Department of Meteorology, University of Maryland, College Park, MD 20742, USA. (senya@atmos.umd.edu)

G. R. Foltz and M. J. McPhaden, NOAA/Pacific Marine Environmental Laboratory, 7600 Sand Point Way NE, Seattle, WA 98115, USA.